

# High-energy density graphite/AC capacitor in organic electrolyte

V. Khomenko<sup>a,b</sup>, E. Raymundo-Piñero<sup>a</sup>, F. Béguin<sup>a,\*</sup>

<sup>a</sup> Centre de Recherche sur la Matière Divisée, CNRS-University, 1B rue de la Férollerie, 45071 Orléans Cedex 2, France

<sup>b</sup> Kiev National University of Technologies & Design, 2 Nemirovich-Danchenko street, Kiev 02011, Ukraine

Received 11 September 2007; received in revised form 11 November 2007; accepted 25 November 2007

Available online 5 December 2007

## Abstract

A high-energy density hybrid capacitor has been designed in organic electrolyte (1 mol L<sup>-1</sup> LiPF<sub>6</sub> in 1:1 ethylene carbonate (EC)/dimethyl carbonate (DMC)) using commercial grades of graphite and activated carbon for negative and positive electrodes, respectively. Different approaches have been explored for assembling the hybrid capacitor in order to achieve an optimum ratio between the energy and power density, while keeping a long cycle-life capability. In the optimized hybrid capacitor, the potential of the positive electrode ranges from 1.5 up to 5 V vs. Li/Li<sup>+</sup>, being extended to the whole stability window of the activated carbon in the organic electrolyte, whereas the potential of the negative electrode remains almost constant at around 0.1 V vs. Li/Li<sup>+</sup>. After balancing carefully the respective masses of the electrodes and appropriately formatting the system, it was found that a voltage of 4.5 V is the optimal value for avoiding a capacitance fading of the hybrid capacitor during cycling. Gravimetric and volumetric energy densities as high as 103.8 Wh kg<sup>-1</sup> and 111.8 Wh L<sup>-1</sup>, respectively, were obtained. The noticeable value of volumetric energy density is 10 times higher than for symmetric or asymmetric capacitors built with the same activated carbon.

© 2007 Elsevier B.V. All rights reserved.

**Keywords:** Electrochemical capacitor; Hybrid capacitor; Lithium intercalation electrode; Electrical double layer; Activated carbon; Graphite

## 1. Introduction

In comparison with the different energy storage devices which can be found in the market, batteries show the highest energy density (150–200 Wh kg<sup>-1</sup>), and they can be engineered for delivering power up to 1000 W kg<sup>-1</sup> [1]. However, they have a limited cycle-life (usually less than 1000 cycles). On the other hand, electrochemical capacitors based on activated carbons, so-called supercapacitors, can develop a longer cycle-life (usually higher than 100,000), very high-specific power (above 1000 W kg<sup>-1</sup>) but lower energy density (up to 10 Wh kg<sup>-1</sup>) than batteries [2–4].

The amount of electrical energy accumulated in an electrochemical capacitor is proportional to the capacitance of the electrode material and to the square of working voltage. Since the operating voltage is limited by the electrolyte decomposition, many studies are focused on using organic electrolytes, considering that they can theoretically reach over 3 V. However, in

practice, supercapacitors based on activated carbon (AC) using Et<sub>4</sub>NBF<sub>4</sub> in acetonitrile (AN) or propylene carbonate as organic electrolyte are able to operate only up to 2.7 V [2].

Generally, in an electrochemical double-layer capacitor, the positive and negative electrodes are identical. In order to increase the energy density while keeping a long cycle-life and a fast charge capability, asymmetric cells consisting of different type of positive and negative electrodes have been introduced. Very interesting results have been attained in aqueous electrolyte with a hybrid configuration combining one electrode made from activated carbon and another containing nickel oxide [5,6], lead oxide [7,8], manganese oxide [9,10] or electronically conducting polymers [11,12]. Amatucci et al. [13,14] have developed a non-aqueous hybrid device by using a Li intercalation negative electrode based on nanostructured Li<sub>4</sub>Ti<sub>5</sub>O<sub>12</sub> and activated carbon as electrical double-layer positive electrode. Following this idea, other examples of hybrid capacitors using titanium-based compounds have been further published [15,16]. Regarding these studies, it should be noted that intercalation–deintercalation in Li<sub>4</sub>Ti<sub>5</sub>O<sub>12</sub>-based materials takes place at around 1.5 V vs. Li. In such conditions, the hybrid capacitor could be only charged–discharged between 1.2 and

\* Corresponding author.

E-mail address: [beguin@cnrs-orleans.fr](mailto:beguin@cnrs-orleans.fr) (F. Béguin).

3.2 V, leading to under using of the positive electrode. Therefore, another approach should be explored for extending the operating voltage of such kind of hybrid capacitor.

From the Li-ion battery technology, it is known that carbon materials can be intercalated by lithium at more negative potentials. In commercial Li-ion batteries, two kinds of carbon materials are mainly used as negative electrode: (i) hard carbon and (ii) graphite. There are some disadvantages of hard carbon (HC) as compared with graphite: (i) HC has very poor rate performance related to a slow diffusion of lithium in the internal carbon structure; (ii) the HC charge–discharge curve is not flat and the potential gradually varies during the deintercalation–intercalation process; (iii) HC has a large initial irreversible capacity [17]. Graphite-based electrodes have not the above-mentioned disadvantages and they are considered as the best choice for the negative electrode of lithium-ion batteries [1,18,19].

The idea here is to develop a hybrid system in organic electrolyte, using graphite and activated carbon as negative and positive electrode materials, respectively. The detailed steps allowing this system to be optimized are presented in this paper.

## 2. Experimental

Commercial activated carbons (AC) including SUPER 50 (Norit) and Maxsorb (Kansai) and two grades of natural graphite SLC1025 and LBG73 provided by Superior Graphite Co., USA, were selected for the present study. Electrodes were prepared by following the standard procedure used in the lithium-ion battery industry [25]. The active materials are first mixed with 5–10 wt% binder (PVDF) dissolved in *N*-methylpyrrolidone (NMP). This mixture is cast onto a 0.015 mm thickness metal foil. Copper and aluminum foils were used for graphite and activated carbon-based electrodes, respectively. After evaporation of the solvent (NMP), the electrodes are dried at 120 °C overnight under primary vacuum. Then the electrodes are compacted to the desired density by roll milling. The active loadings of graphite and activated carbon were in the range of 2–6 mg cm<sup>-2</sup>, giving active layers with thicknesses in the range 0.04–0.10 mm. Disc electrodes having a diameter of 11.5 mm were cut out by punching the coating film cast onto the metal foil current collector. Two electrode capacitors were built with a glassy fibrous separator, using a Teflon Swagelok® type system. Two electrolytic solutions have been studied: 1 mol L<sup>-1</sup> Et<sub>4</sub>NBF<sub>4</sub> in acetonitrile (AN) and 1 mol L<sup>-1</sup> LiPF<sub>6</sub> in a mixture of ethylene carbonate (EC) and dimethyl carbonate (DMC).

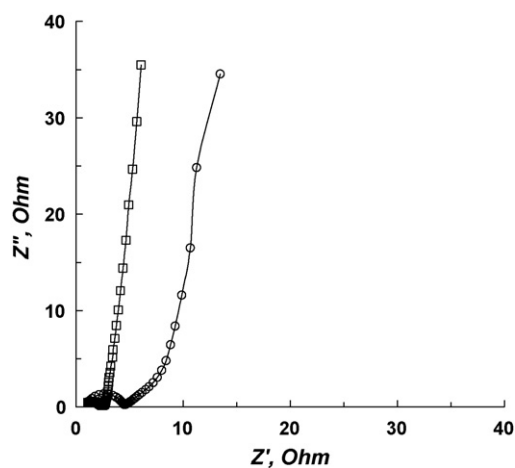


Fig. 1. Impedance spectra of electrical double-layer capacitors based on the activated carbons Maxsorb (○) and Super 50 (□) using 1 mol L<sup>-1</sup> Et<sub>4</sub>NBF<sub>4</sub> in AN.

To evaluate the electrochemical properties of the electrodes, experiments were also performed using a Li disk as reference and counter electrode. All the potentials in the manuscript are presented vs. the Li electrode. The electrochemical characteristics of the electrode and capacitor were determined by cyclic voltammetry, galvanostatic charge–discharge cycling and impedance spectroscopy measurements using a VMP2 (Biologic, France) multichannel generator.

## 3. Results and discussion

### 3.1. Electrochemical performance of activated carbon

Two different commercial activated carbons have been studied: Super 50 (Norit) and Maxsorb (Kansai). From Table 1, it can be observed that they contain the same amount of oxygen on their surface but the porous texture is completely different. The activated carbon Maxsorb has a very developed surface area with a wide pore size distribution, whereas Super 50 presents a lower surface area and a narrower pore size distribution with most of the porosity in the range of micropores.

These two ACs were firstly tested in symmetric capacitors built in 1 mol L<sup>-1</sup> Et<sub>4</sub>NBF<sub>4</sub> in AN. Fig. 1 shows the impedance spectra for the two supercapacitors which have almost the same composition in terms of binder and mass of electrodes. In the low-frequency regime, both capacitors show an ideal capacitive behavior, with a near vertical line parallel to the imaginary axis. The capacitance values are 76 and 150 F g<sup>-1</sup>, and the

Table 1  
Porous texture and oxygen content of the activated carbons

Sample	$S_{\text{BET}} (\text{N}_2)$ (m <sup>2</sup> g <sup>-1</sup> )	$S_{\text{DR}} (\text{CO}_2)$ (m <sup>2</sup> g <sup>-1</sup> )	$V_{\text{ultramicro}}^{\text{a}}$ $d < 0.7$ nm (cm <sup>3</sup> g <sup>-1</sup> )	$V_{\text{micro}}^{\text{b}}$ $0.7 < d < 2$ nm (cm <sup>3</sup> g <sup>-1</sup> )	$V_{\text{meso}}^{\text{b}}$ $2 < d < 50$ nm (cm <sup>3</sup> g <sup>-1</sup> )	O (at%)
Maxsorb	3487	1754	0.67	0.77	0.86	5.0
Super 50	1402	1283	0.49	0.36	0.21	4.6

<sup>a</sup> Obtained after applying the Dubinin–Radushkevich equation to the CO<sub>2</sub> adsorption data.

<sup>b</sup> Obtained after applying the DFT method to the N<sub>2</sub> adsorption data.

equivalent series resistance (ESR) 2.6 and  $4.7 \Omega \text{ cm}^2$  for the capacitors based on Super 50 and Maxsorb, respectively. Taking into account that Maxsorb is the most capacitive but also the most resistive carbon, Super 50 could be preferable for engineering high-power capacitors. Additionally, since Super 50 is less porous than Maxsorb, the electrode density with Super 50 is  $0.79 \text{ g cm}^{-3}$  and only  $0.37 \text{ g cm}^{-3}$  when using Maxsorb. Consequently, Super 50 displays a higher volumetric capacitance than Maxsorb, being more attractive for the development of compact size capacitors.

Another limitation presented by high-surface area carbon materials is the long-term stability of the capacitor. The higher the specific surface area of an AC, the higher the active surface area (ASA) and the higher the risk of electrolyte decomposition. Fig. 2 shows the galvanostatic charge–discharge cycling for the two carbon-based capacitors at a maximum cell voltage of 2.5 and 3.0 V. It is clearly observable that the Maxsorb-based capacitor presents an important capacitance fading, whatever the cell voltage applied, due to the decomposition of the electrolyte [29]. In conclusion, considering these results, we have selected AC Super 50 as the most suitable for further investigation in organic electrolyte.

Keeping in mind the idea of using AC as positive electrode in a hybrid configuration where the negative electrode will work as a Li intercalation compound, the electrochemical characteristics of the selected activated carbon were investigated using a lithium-based organic electrolyte ( $1 \text{ mol L}^{-1} \text{ LiPF}_6$  in EC/DMC). Fig. 3 shows the cyclic voltammograms obtained with different potential ranges in a three-electrode cell where Super 50 is the working electrode and metallic Li is used as reference and counter electrode. In the range from 2.0 to 4.0 V vs. Li, the rectangular voltammogram with a mirror symmetry image of the current response from the zero current line is typical of charging a double layer. If the potential range is extended down to potentials smaller than 1.0 V vs. Li, e.g., 0.5 V, the response is different. As it is shown in Fig. 3, such a polarization leads to a decrease of the specific capacitance together with a remarkable change of behavior in the range from 2.0 to 4.0 V. At low potential, the electrolyte is decomposed and a solid electrolyte interphase (S.E.I.) is formed on the surface of activated carbon,

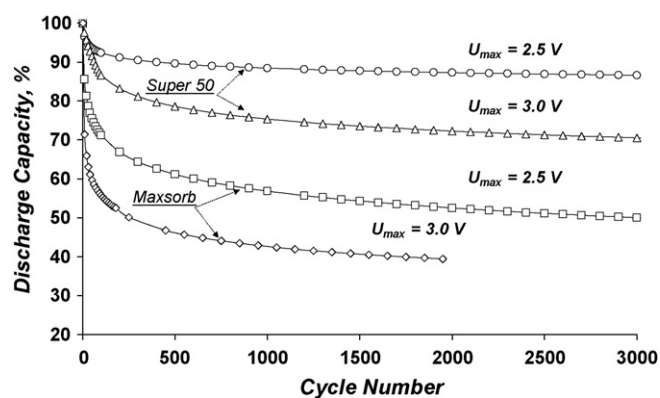


Fig. 2. Cycle-life of electrical double-layer capacitors based on Super 50 (○; △) and Maxsorb (□; ◇) using  $1 \text{ mol L}^{-1} \text{ Et}_4\text{NBF}_4$  in AN. The cells are cycled with different cut-off voltage ( $U_{\text{max}}$ ) at a current density of  $650 \text{ mA g}^{-1}$ .

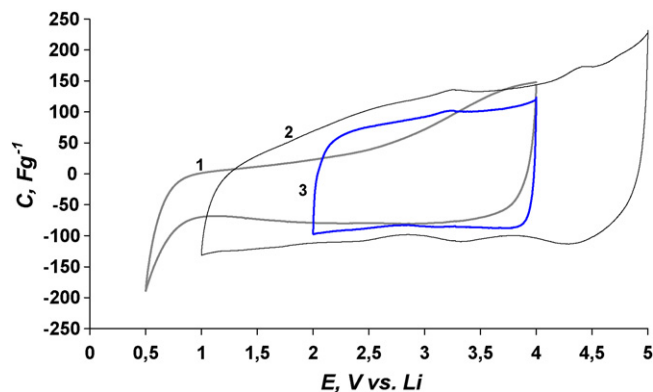


Fig. 3. Cyclic voltammograms of the activated carbon Super 50 in a three-electrode cell at  $5 \text{ mV s}^{-1}$  using  $1 \text{ mol L}^{-1} \text{ LiPF}_6$  in EC/DMC as electrolyte. Potential range: (1) 0.5–4.0 V; (2) 1.0–5.0 V; (3) 2.0–4.0 V.

as it happens on the negative electrode of a lithium-ion battery during the formation cycle [20,21]. It seems that the S.E.I. products block the pores of the AC, limiting a further access of the electrolyte ions to the active surface. In the other sense of polarization, the limit for irreversible processes was observed only above 5.0 V vs. Li. The later observation well agrees with tests on cathode materials for lithium-ion batteries, showing that the electrolyte is stable at a nominal voltage of 5 V [30].

From Fig. 3 it is also clearly seen that the capacitance increases with increasing the potential window of the CV scan. In the potential range from 1.0 to 5.0 V, even if the voltammogram becomes far from the ideal capacitive one, the reversible charge–discharge capacitance is higher than in the range from 2.0 to 4.0 V. In order to elucidate the reason of this capacitance dependence, galvanostatic charge–discharge tests were performed in the narrow (2.0–4.0 V) and wide (1.0–5.0 V) range of potential (Fig. 4). The discharge curves are almost linear in the two ranges of potential, whereas the charge one is out of linearity in the range 1.0–1.5 V. The capacitance values obtained from the discharge characteristics of the activated carbon are 86 and  $114 \text{ F g}^{-1}$  in the narrow and wide ranges of potential, respectively. The Coulomb efficiencies are about 99 and 95% for the narrow and wide potential range, respectively. The higher value

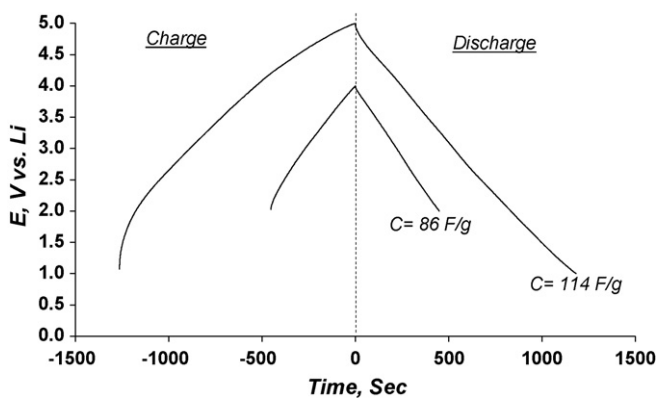


Fig. 4. Galvanostatic charge–discharge profile of the activated carbon Super 50 in a three-electrode cell using  $1 \text{ mol L}^{-1} \text{ LiPF}_6$  in EC/DMC. The current density is  $385 \text{ mA g}^{-1}$  of activated carbon.

of capacitance could be due to the contribution of  $\text{Li}^+$  and  $\text{PF}_6^-$  intercalation in some graphitic type stackings [22,23]. In summary, from the data presented in Figs. 3 and 4, it is possible to suggest that the operating potential range for activated carbon should be higher than 1.0 V and lower than 5.0 V vs.  $\text{Li}/\text{Li}^+$ .

### 3.2. Electrochemical performance of graphite

The performance of thermally purified natural crystalline graphite either with almost spherical “potato shape” (SLC1025) particles or with planar or “prismatic shape” (LBG73) particles has been studied at various current densities in a cell using a Li metal counter electrode. The reversible capacity obtained for both types of graphite (SLC1025 and LBG73) at a current rate of  $C/20$  was  $352 \text{ mA h g}^{-1}$  within the potential range 0.01–1.5 V (Fig. 5, inset). The irreversible capacity was 28 and  $37 \text{ mA h g}^{-1}$  for SLC1025 and LBG73, respectively. At the second and subsequent cycles, both graphites show a good reversibility with a Coulombic efficiency close to 100%. However, it is well known that the reversible specific capacity decreases when increasing the current rate. In this sense, Fig. 5 shows the composition of the intercalated graphite,  $x$  in  $\text{Li}_x\text{C}_6$ , obtained as a function of the discharge rate. At low current, the composition of lithiated graphite approaches the theoretical value,  $x \sim 1$ , in both materials. As the specific current increases,  $x$  decreases more rapidly for the prismatic graphite than for the potato-shape one. This trend suggests that the solid-state diffusion of Li ions limits the intercalation in the flake-like structure. It can be found in the literature [24] that lithium intercalation occurs mainly at the edge sites of graphite. Therefore, changing the morphology of the particles from 2D (flake) to 3D (potato shape) allows a higher capacity to be obtained at high-current rate.

### 3.3. Design and optimization of a hybrid capacitor-based on activated carbon and graphite

From the information obtained above, a hybrid cell is designed in  $1 \text{ mol L}^{-1} \text{ LiPF}_6$  in EC/DMC 1:1 by combining

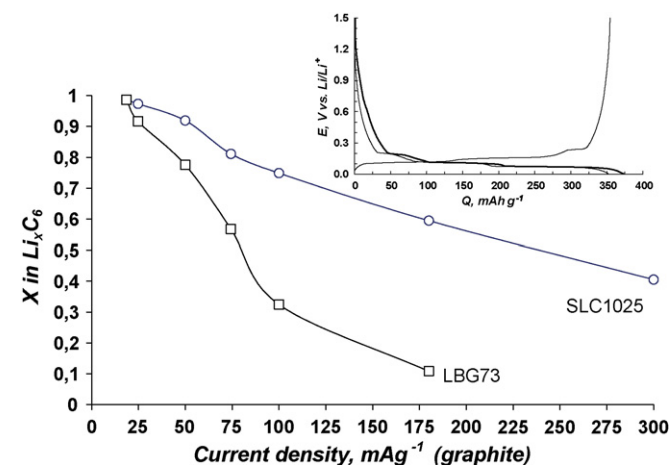


Fig. 5. Effect of current density on the reversible capacity of natural graphite with prismatic ( $\square$  LBG73) and potato ( $\circ$  SLC1025) shape of particles. The inset shows the galvanostatic charge–discharge profile of graphite at a rate  $C/20$ .

graphite (SLC1025) and activated carbon (Super 50) as negative and positive electrode, respectively. In order to ensure a high-energy density with such a hybrid device, the mass of the electrodes should be balanced to fully take profit of the performance of both materials in their optimal working potential range. For this purpose, the charge passing through the positive ( $Q_{\text{AC}}$ ) and the negative ( $Q_{\text{graphite}}$ ) electrodes should be balanced. The charge stored in each electrode depends on the specific capacitance ( $C$ ), the potential range for the charge–discharge process ( $\Delta E$ ) and the mass of the electrode ( $m$ ) following the relationship:  $Q = C \cdot \Delta E \cdot m$ . From the data presented in previous sections, the specific capacitance of activated carbon is about  $90 \text{ F g}^{-1}$ , which corresponds to a specific capacity of  $\sim 75 \text{ mA h g}^{-1}$  in the range of potential from 2.0 to 5.0 V. The specific capacity of graphite is about  $380 \text{ mA h g}^{-1}$  (after adding  $28 \text{ mA h g}^{-1}$  of irreversible capacity). Thus, in order to get  $Q_{\text{AC}} = Q_{\text{graphite}}$ , the mass ratio AC:graphite should be 5:1. Upon charging a hybrid capacitor built with this ratio, the graphite negative electrode will be fully lithiated, whereas the AC positive electrode will be charged–discharged in the potential range from 2.0 to 5.0 V.

Fig. 6 shows the galvanostatic charge–discharge profile of the hybrid cell assembled with this mass ratio in the voltage range from 0.0 to 5.0 V at a current rate  $C$ . The potential of the positive and negative electrodes has been recorded separately vs. a Li reference electrode during the charge–discharge of the cell. In the figure, it can be observed that the operating conditions of both electrodes are optimized, allowing graphite to be fully intercalated. However, since the charge storage in graphite occurs through reversible lithium intercalation, it is obvious that the performance, e.g., the power of the cell, will be limited by the negative electrode. Additionally, the lowest value of potential for lithium intercalation into graphite is very close to the lithium plating potential. Taking into account that lithium plating is undesirable for a long cycle-life of the hybrid capacitor, the graphite electrode should not be polarized until reaching the total capacity of graphite, i.e., until complete lithiation to  $\text{LiC}_6$ . For protecting the graphite electrode from this phenomenon, the effective equivalent weight of the graphite

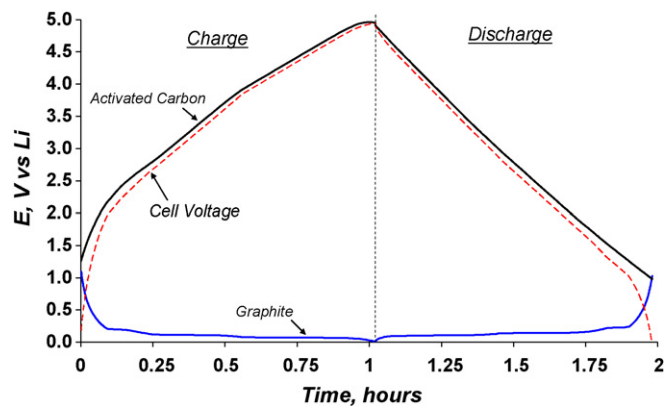


Fig. 6. Galvanostatic charge–discharge at a current density  $C$  of the electrodes and cell (dotted line) for a hybrid capacitor utilizing activated carbon as positive electrode and graphite as negative electrode. The cell was assembled with a mass ratio:  $m$  (activated carbon)/ $m$  (graphite) = 5/1.

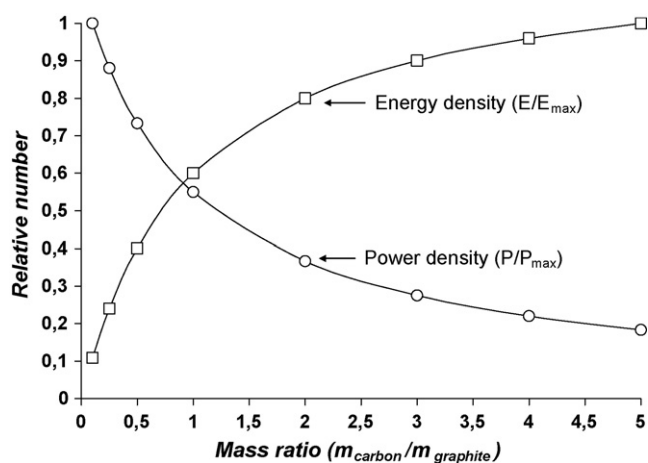


Fig. 7. Relative power and energy density as a function of the mass ratio of the electrodes for hybrid capacitors utilizing activated carbon as positive electrode and graphite as negative electrode.

electrode should be increased in comparison to the weight of the activated carbon-based electrode. It results clearly that the mass ratio (AC:graphite) should be optimized in order to achieve high energy and power density with a long cycle-life.

Our initial estimation indicated a maximum value of energy density ( $E_{\max}$ ) for a mass ratio AC/graphite = 5/1. Fig. 7 shows the relative energy  $E/E_{\max}$  obtained after keeping constant the mass of the AC electrode and increasing the mass of graphite electrode in a cell working with a maximum voltage of 5.0 V. As it was expected, the energy density decreases when the mass ratio AC/graphite decreases, being this phenomenon faster for ratios smaller than 2.

The power density itself is expressed by the equation  $P_{\max} = V^2/4R$ . From the time constant  $\tau = RC$ , where  $R$  and  $C$  are the series resistance and capacitance of cell, respectively, it comes that  $P = E/2\tau$ . The time constant of the hybrid device is obviously limited by the graphite electrode. Electrochemical lithium intercalation into graphite involves a variety of processes such as diffusion in the electrolyte solution, migration through the surface film, charge transfer at the graphite–electrolyte interface and diffusion within the graphite electrode. Because the diffusion in a solid is generally a slow process, we suggest that the diffusion rate controls the time constant. For a spherical particle, the time constant is given by  $\tau = l^2/D$ , where  $l$  is the diameter of the particle and  $D$  is the diffusion coefficient of Li into graphite. In previous studies [26,27], the value of this coefficient has been estimated as about  $2 \times 10^{-8} \text{ cm}^2 \text{ s}^{-1}$ . Taking into account that the average particle size of the graphite SLC1025 is 26  $\mu\text{m}$ , the time constant for a complete intercalation of the graphite electrode is 338 s. Then, one can calculate the power  $P_0$  related with the maximum energy value  $E_{\max}$  (at mass ratio 5/1) by applying the equation  $P = E/2\tau$ . For the other values of mass ratio, the power  $P$  is also calculated using the same equation where  $E$  is the corresponding value of energy at this mass ratio. The plot of the relative power density,  $P/P_0$  vs. the mass ratio of the electrodes in Fig. 7 shows that increasing the mass of the graphite electrode in the hybrid capacitor leads to an increase in the relative power, with a maximum at a mass

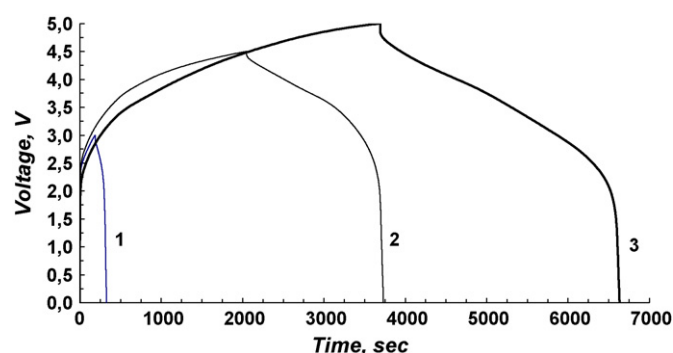


Fig. 8. Charge–discharge profiles at different values of cut-off voltage (1.0–3.0 V; 2.0–4.5 V; 3.0–5.0 V) for a hybrid capacitor utilizing activated carbon as positive electrode and graphite as negative electrode. The cell was assembled with a mass ratio:  $m$  (activated carbon)/ $m$  (graphite) = 1/1.

ratio 1:1. This decrease of time constant is due to a decrease in the depth of Li intercalation when the mass of graphite increases. As a conclusion, considering that a capacitor must be essentially a power device, the best compromise between energy and power is obtained for an electrode mass ratio of 1:1.

After selecting the electrode mass ratio, other parameters should be studied in order to optimize the performance of the hybrid device. One of the most influencing ones is the cell voltage. For illustration, Fig. 8 shows the galvanostatic charge–discharge profiles obtained at different voltage ranges for a hybrid cell assembled with an electrode mass ratio of 1:1. As the maximum cell voltage increases from 3.0 to 5.0 V, the capacitance of the hybrid device increases. However, in each case, the maximum charge is only delivered from voltages higher than 2.0 V. Such a behavior could be predicted after observing the inset in Fig. 5. The capacity of the graphite electrode is very low in the range of potentials from 2.0 to 0.2 V vs. Li. Therefore, the potential of the graphite electrode in the hybrid device sharply falls to 0.2 V during the charge of the capacitor and it sharply increases up to 2.0 V during the discharge of the cell. Thus, considering that the voltage of the hybrid capacitor is the difference between the potential increment of the positive electrode and the potential increment of the negative one ( $\Delta U = \Delta E^+ - \Delta E^-$ ), the potential variation of the graphite electrode will determine the voltage of the cell in the range between 0.0 and 2.0 V. In conclusion, for obtaining a hybrid cell where the electrochemical behavior will be controlled by the AC electrode, the working potential range of the graphite electrode should be located below 0.2 V vs. Li/Li<sup>+</sup>. For this purpose, cycling the hybrid cell should start from 1.5 V instead of 0.0 V.

Fig. 9 shows the long-term stability test of the hybrid capacitor performed using a voltage range between 1.5 and 4.5 V. At the beginning of cycling, the capacitance of the device was about 35% of the value which can be obtained with activated carbon in the range of potential from 1.5 to 4.5 V, as it was estimated in previous experiments (see Section 3.1). After 300 charge–discharge cycles, the hybrid capacitor presents its maximal capacitance, which is only 84% of the value for activated carbon, and an important fade of capacitance is observed after 500 cycles. Hence, it seems that the graphite electrode is still determining the capacitance of the hybrid capacitor. Both elec-

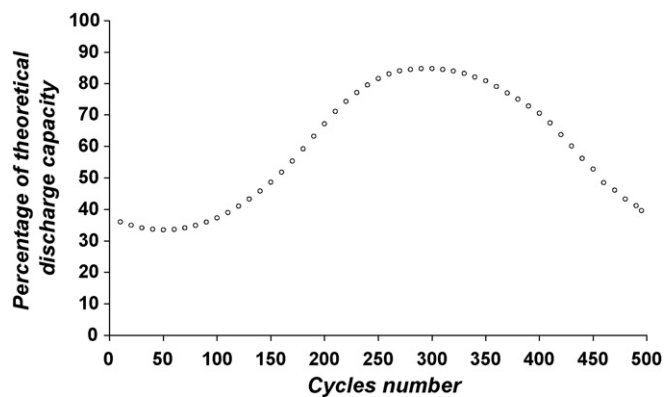


Fig. 9. Cycle-life of a hybrid capacitor utilizing activated carbon as positive electrode and graphite as negative electrode. The cell was assembled with a mass ratio:  $m$  (activated carbon)/ $m$  (graphite) = 1/1. The theoretical discharge capacity of the hybrid capacitor was estimated taking into account the mass and specific capacity of activated carbon.

trodes are operating out of their stability potential window; in particular the operating potential range of the graphite electrode is probably higher than 0.2 V vs. Li/Li<sup>+</sup>.

Therefore, with the idea of overcoming the previous under-performance, a special procedure comprising some “formation cycles” has been designed in order to shift the potential of the graphite electrode to lower values. After the cell was charged at a current rate of  $C/20$  up to a given voltage, it was allowed to relax at open circuit for three hours. Then the cell was charged up to a higher voltage, followed by relaxation, and so on. Fig. 10 shows together the variation of cell voltage and potential of the graphite electrode vs. time during the designed formation cycles at incrementing maximum cell voltage. It can be seen that after a charge up to 4.0 V, the cell voltage falls down to 3.5 V during the relaxation period, whereas the potential change of the graphite

electrode is less than 50 mV. In that point, it is necessary to recall that the overall self-discharge of a capacitor is the sum of the individual self-discharges taking place at each electrode in opposite directions. As stated by Amatucci and coworkers [28], the AC-based electrode has a higher self-discharge rate than the redox graphite one and it consequently determines the self-discharge rate of the hybrid capacitor. These differences in the rate of self-discharge will allow to achieve the desired potential of 0.1 V vs. Li/Li<sup>+</sup> for the graphite electrode after a series of charge cycles at increasing cell voltage, e.g., 4.3 and 4.5 V, followed by 3 h relaxation periods. After such formation cycles, the potential of the graphite electrode becomes stable and the capacitor can be charged–discharged with an almost ideal linear profile as it can be seen for the last cycles in Fig. 10. We assume that the formation of the highly resistive S.E.I. during the first cycles at increasing voltage is at the origin of the potential down shift of the graphite electrode.

In conclusion, with such a simple procedure, an optimal behavior of the hybrid capacitor can be accomplished. For a better illustration, Fig. 11 shows the galvanostatic charge and discharge curves of the hybrid capacitor, after the formation cycles, at a current density of 650 mA g<sup>-1</sup> in 1 mol L<sup>-1</sup> LiPF<sub>6</sub> in EC/DMC. The cell shows almost linear discharge characteristics in the voltage range of 1.5–4.5 V. The confirmation of the optimized behavior of the hybrid capacitor can be obtained after recording the potential changes of the negative and positive electrodes during the charge–discharge of the cell, using a Li reference electrode. The potential changes for the graphite electrode were very small and in the very desirable window of 0.10–0.16 V vs. Li/Li<sup>+</sup> (see inset in Fig. 11). Simultaneously, the potential of the activated carbon electrode changes in the range of 4.6 to 1.66 V vs. Li/Li<sup>+</sup>. Therefore, now it is clear that the charge–discharge characteristics of the hybrid cell are largely regulated by the activated carbon elec-

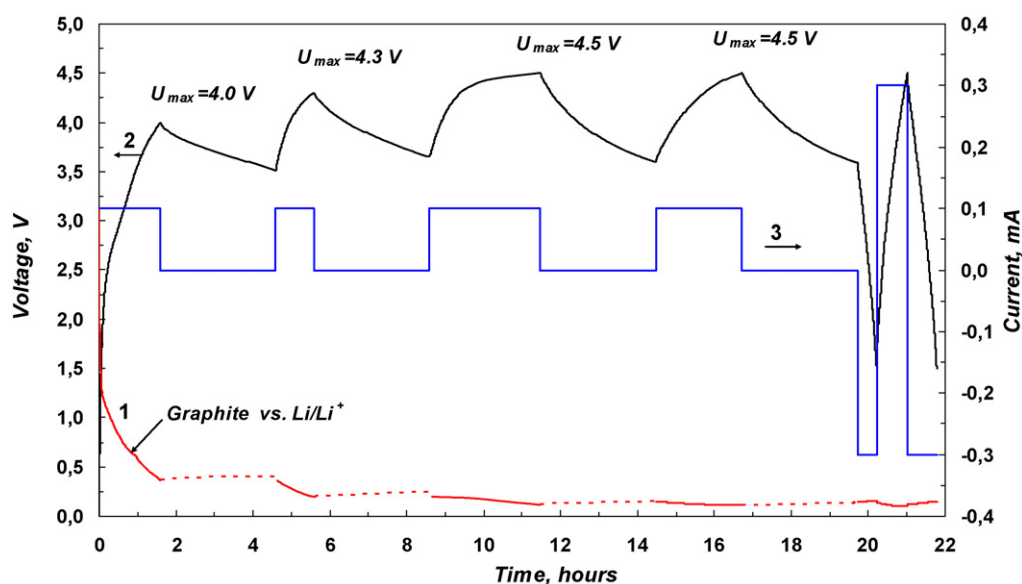


Fig. 10. Charge–discharge voltage (2) and current (3) profiles of the hybrid capacitor during formation cycles at a current rate  $C/20$ . The curve (1) represents the potential variation of the graphite electrode, whereas the dotted line corresponds to the relaxation periods between charge cycles. The cell was assembled with a mass ratio:  $m$  (activated carbon)/ $m$  (graphite) = 1/1.

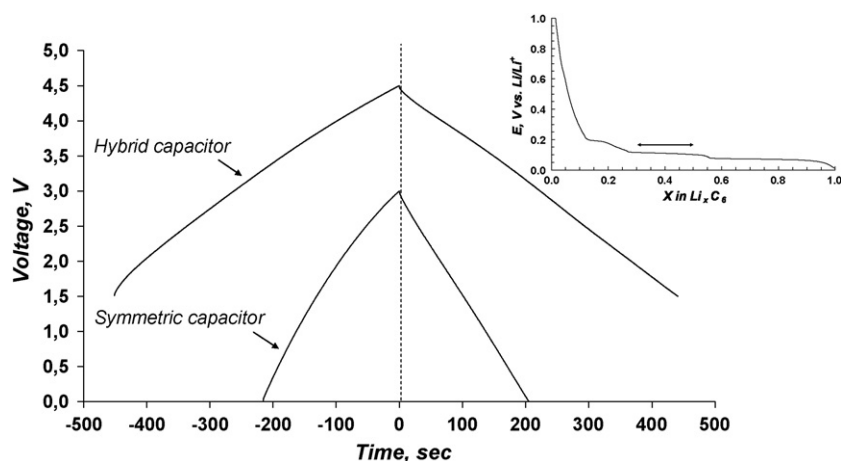


Fig. 11. Cell output voltage comparison for one charge–discharge cycle of symmetric (both electrodes based on activated carbon) and hybrid capacitors using the same electrolyte ( $1 \text{ mol L}^{-1} \text{ LiPF}_6$  in EC/DMC) and electrodes mass loading. The inset shows the potential and capacity range (arrow) of the graphite electrode during the charge–discharge of the hybrid capacitor between 1.5 and 4.5 V.

trode due to its lower capacitance in comparison to the graphite one.

In order to obtain information concerning the long-term stability of the hybrid device, charge–discharge cycles were performed at different cell voltages. Fig. 12 shows the discharge capacitance as a function of the cycle number for a charge–discharge cycling at a current density of  $650 \text{ mA g}^{-1}$  using maximum cell voltages of 4.5, 4.7 and 5.0 V. Applying a maximum cut-off voltage of 4.7 and 5.0 V turns after 10,000 cycles to a capacitance fade of  $\sim 75$  and  $\sim 60\%$  of the initial value, respectively. By contrast, a very good stability is observed when using a maximum cut-off voltage of 4.5 V. Over 86% of the initial discharge capacitance can be kept after 10,000 cycles. It should be noted that the main capacitance fading appears in the beginning of cycling. The capacitance decreases to  $\sim 88\%$  of the initial value during the first  $\sim 100$  cycles, remaining constant during the rest of the cycling test. This capacitance fade still has to be clarified, but it is probably due to changes in the operating potential range of the carbon electrode. As it was presented before (see Figs. 3 and 4), the capacitance of the carbon electrode depends on its working potential range.

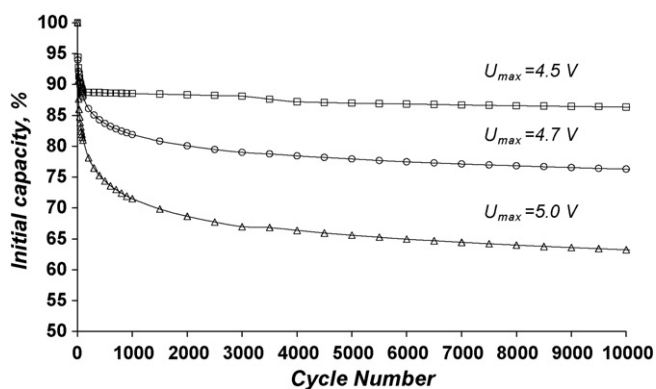


Fig. 12. Cycle-life of hybrid capacitors cycled between 1.5 V and different maximum cut-off voltage ( $U_{\text{max}}$ ) at a current density of  $650 \text{ mA g}^{-1}$  (per mass of one electrode). The cells were assembled with mass a ratio:  $m$  (activated carbon)/ $m$  (graphite) = 1/1.

From the results presented above, we can conclude that a cell voltage between 1.5 and 4.5 V is optimal for obtaining the best performance of the hybrid capacitor, while avoiding a capacitance fading during cycling.

### 3.4. Performance comparison between the hybrid and symmetric capacitor

Fig. 11 presents the galvanostatic charge–discharge curve obtained at  $650 \text{ mA g}^{-1}$  for a symmetric capacitor prepared with two AC electrodes in comparison with the results for the hybrid capacitor discussed above. Both capacitors were prepared using the same mass of electrodes. The two different capacitors show almost linear charge–discharge characteristics with a Coulombic efficiency of about 98 and 95% for the hybrid and the symmetric capacitor, respectively. From the discharge curves, it was calculated that the discharge capacitance of the hybrid capacitor (120 mF) is two times higher than for the symmetric one (60 mF). From this data, it results clearly that the capacitance of the cell can be markedly increased by replacing one of the acti-

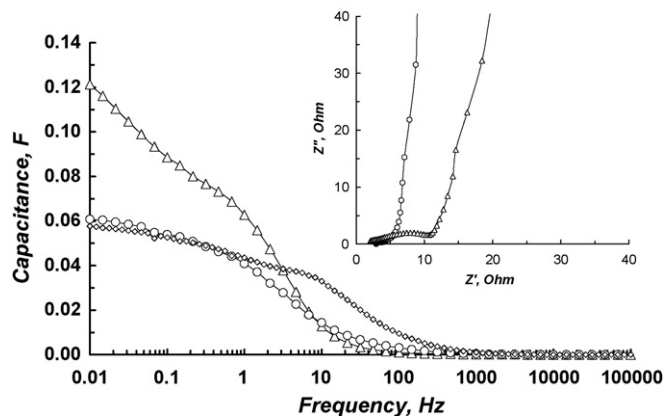


Fig. 13. Impedance spectra of the hybrid capacitor ( $\Delta$ ) and of symmetric capacitors based on  $1 \text{ mol L}^{-1} \text{ LiPF}_6$  in EC/DMC ( $\circ$ ) and  $1 \text{ mol L}^{-1} \text{ Et}_4\text{NBF}_4$  in AN ( $\diamond$ ). All capacitors were assembled with the same electrodes mass loading.

Table 2  
Electrochemical performance of the symmetric and hybrid capacitors based on various organic electrolytes

Type of cell	Electrolyte	Cell voltage (V)	ESR ( $\Omega$ ) (100 kHz)	EDR ( $\Omega$ ) (1 Hz)	$P_{\max}^a$ ( $\text{kW kg}^{-1}$ )	Specific energy <sup>a</sup>	
						( $\text{Wh kg}^{-1}$ )	( $\text{Wh L}^{-1}$ )
Symmetric	$\text{Et}_4\text{NBF}_4$ in AN	2.5	2.1	3.2	32	17.2	9.8
Symmetric	$\text{LiPF}_6$ in EC/DMC	3.0	3.1	6.0	5.5	22.6	12.9
Hybrid	$\text{LiPF}_6$ in EC/DMC	5.0	3.3	11.8	10	145.8	157.5
Hybrid	$\text{LiPF}_6$ in EC/DMC	4.5	3.3	11.8	10	103.8	111.8

<sup>a</sup> Specific energy and power calculated for the total mass of electrodes.

vated carbon electrodes by a graphite-based one. Another great advantage of the hybrid device is that it can operate at higher cell voltage than a symmetric system in the same electrolyte.

Electrochemical impedance spectroscopy is an extremely useful tool for comparing electrochemical capacitors. With this technique, the capacitance and the contribution to the electrical series resistance (ESR) can be determined. Fig. 13 shows the plot of capacitance  $C = 1/(\omega \text{Im} Z)$  as a function of frequency for three different capacitors: (i) symmetric double-layer capacitor assembled in  $1 \text{ mol L}^{-1} \text{ Et}_4\text{NBF}_4$  in AN (this electrolyte is the most commonly used for commercial supercapacitors), (ii) symmetric double-layer capacitor assembled in  $1 \text{ mol L}^{-1} \text{ LiPF}_6$  in EC/DMC and (iii) hybrid capacitor assembled in  $1 \text{ mol L}^{-1} \text{ LiPF}_6$  in EC/DMC. The inset of Fig. 13 presents the Nyquist plots for the capacitors (ii) and (iii) (the Nyquist plot of the capacitor (i) has been already presented in Fig. 1). At high frequencies, the Nyquist plots demonstrate that all capacitors behave almost like a simple resistor. In contrary, for low frequencies, all the spectra approach to a vertical line, behaving almost like an ideal RC series connection, with R and C being no longer frequency-dependent. Comparing the symmetric capacitor in  $\text{Et}_4\text{NBF}_4$  (see Fig. 1) and in  $\text{LiPF}_6$  (Fig. 13, inset), it can be seen that the resistance of the second one is higher. It is obvious that the use of  $1 \text{ mol L}^{-1} \text{ LiPF}_6$  in EC/DMC as electrolyte for a supercapacitor introduces some loss in performance due its lower conductivity compared to the electrolyte based on AN [1]. Such an increased resistance will have a significant impact on the power capability of the capacitor as it is presented in Table 2. Hence, the use of this electrolyte in the hybrid capacitor will be also detrimental for its conductivity, as it can be observed in the inset of Fig. 13. However, Table 2 shows that the power is higher than for the symmetric capacitor in the same electrolyte.

The capacitance of all types of capacitors decreases with increasing frequency (Fig. 13). The sharpest decreases in capacitance occurs for the symmetric capacitor in the AN-based electrolyte, at about 10 Hz, whereas for the symmetric and hybrid capacitors in the  $\text{LiPF}_6$ -based electrolyte this decrease is less sharp and takes place at  $\sim 1$  Hz. However, it can be clearly seen in the figure that the capacitance of the hybrid capacitor at low frequency is about two times higher than for the two symmetric capacitors. After these results, we can conclude that the hybrid supercapacitor outperforms the symmetric double-layer supercapacitor based on the same electrolyte ( $1 \text{ mol L}^{-1} \text{ LiPF}_6$  in EC/DMC).

All the features extracted from the impedance spectroscopy measurements will be reflected on the performance of the supercapacitors in terms of specific energy and power, particularly at high-current densities. In this sense, Fig. 14 shows the Ragone plots, where the specific energy and average specific power were evaluated from the galvanostatic discharge characteristics at current densities from  $100 \text{ mA g}^{-1}$  to  $100 \text{ A g}^{-1}$  for the hybrid and the two symmetric supercapacitors assembled with the same electrodes mass loading. These data clearly demonstrate that the specific energy of the hybrid supercapacitor is few times higher than for any of the symmetric capacitors. As it can be extracted from Fig. 14, the hybrid capacitor presents a maximum energy of  $145.8 \text{ Wh kg}^{-1}$  in a voltage range from 1.5 V up to 5 V and it can achieve a maximum power of above  $10 \text{ kW kg}^{-1}$ . In the figure, the time constants are also plotted and it becomes obvious that the hybrid capacitor outperforms both symmetric capacitors in terms of specific energy at a working range above 10 s.

Table 2 summarizes the characteristics of all types of capacitors. The results clearly show that the hybrid supercapacitor is more interesting than the electrical double-layer supercapacitors in terms of energy density. Because of the high density of graphite compared to any AC, a volumetric energy density as high as  $157.5 \text{ Wh L}^{-1}$  can be obtained in a voltage range from 1.5 V up to 5 V. Therefore, the hybrid capacitor gives energy densities 15 times higher than the conventional symmetric capacitors. Due to the use of the same graphite materials as in the lithium batteries technology, these hybrid devices

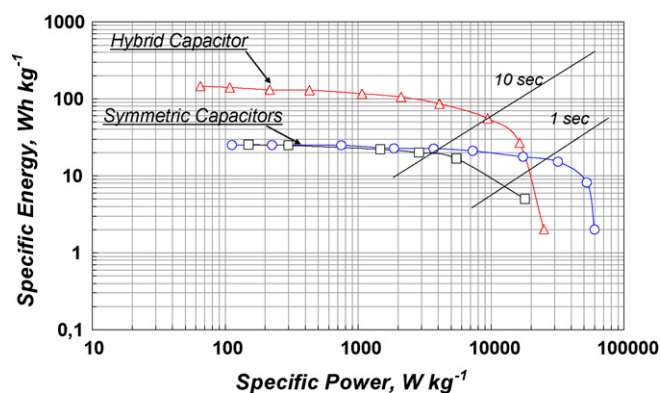


Fig. 14. Ragone plot for the hybrid capacitor ( $\Delta$ ) using  $1 \text{ mol L}^{-1} \text{ LiPF}_6$  in EC/DMC and for the symmetric capacitors using  $1 \text{ mol L}^{-1} \text{ LiPF}_6$  in EC/DMC ( $\square$ ) and  $1 \text{ mol L}^{-1} \text{ Et}_4\text{NBF}_4$  in AN ( $\circ$ ).

can thus provide a positive response to the market demand for high-energy supercapacitors without significantly increasing the costs.

#### 4. Conclusion

A hybrid capacitor has been built by combining commercially available graphite and activated carbon as negative and positive electrodes, respectively. From the experimental data, it was found that the hybrid device can be optimized for working in a voltage range from 1.5 V up to 4.5 V. Additionally, the capacitance of the hybrid capacitor was above 2 times higher than that for a symmetric capacitor. As a consequence, gravimetric and volumetric energy densities as high as  $103.8 \text{ Wh kg}^{-1}$  and  $111.8 \text{ Wh L}^{-1}$  can be obtained in such a hybrid capacitor, while keeping a very good cyclability in a voltage range from 1.5 V up to 4.5 V. The discharge capacitance after 10,000 cycles was over 85% of the initial value, which is much higher than that of any symmetric capacitor operating at a voltage higher than 2.5 V.

#### Acknowledgments

V.K. thanks CNRS for supporting a post-doctoral grant in the frame of the ACI Energie. Thanks are also due to Norit and Superior Graphite for kindly providing AC and graphite samples, respectively.

#### References

- [1] D. Linden, Handbook of Batteries, 2nd ed., McGraw-Hill, New York, 1995.
- [2] B.E. Conway, Electrochemical Supercapacitors: Scientific Fundamentals and Technological Applications, Kluwer Academic Publishers/Plenum Press, New York, 1999.
- [3] A. Burke, J. Power Sources 91 (2000) 37–50.
- [4] E. Frackowiak, F. Béguin, Carbon 39 (2001) 937–950.
- [5] A.L. Beliakov, A.M. Brintsev, Proceedings of the Seventh International Seminar on Double-layer Capacitors and Similar Energy Storage Devices, Deerfield Beach, FL, December 1997.
- [6] S. Razoumov, A. Klementov, S. Litvinenko, A.I. Beliakov, US Patent 6,222,723 (April 24, 2001).
- [7] Y.M. Volkovich, P.A. Shmatko, Proceedings of the Eighth International Seminar on Double-layer Capacitors and Similar Devices, Florida Educational Seminars Inc., Deerfield Beach, FL, 1998.
- [8] W.G. Pell, B.E. Conway, J. Power Sources 136 (2004) 334–345.
- [9] T. Brousse, M. Toupin, D. Bélanger, J. Electrochem. Soc. 151 (2004) A614–A622.
- [10] V. Khomenko, E. Raymundo-Piñero, F. Béguin, J. Power Sources 153 (2006) 183–190.
- [11] C.A. Di Fabio, A. Giorgi, M. Mastragostino, F. Soavi, J. Electrochem. Soc. 148 (2001) A845–A850.
- [12] V. Khomenko, E. Raymundo-Piñero, E. Frackowiak, F. Béguin, Appl. Phys. A: Mater. 82 (2006) 567–573.
- [13] G.G. Amatucci, F. Badway, A. Du Pasquier, T. Zheng, J. Electrochem. Soc. 148 (2001) A930–A939.
- [14] A. Du Pasquier, I. Plitz, J. Gural, S. Menocal, G.G. Amatucci, J. Power Sources 113 (2003) 62–71.
- [15] A. Du Pasquier, I. Plitz, S. Menocal, G.G. Amatucci, J. Power Sources 115 (2003) 171–178.
- [16] T. Brousse, R. Marchand, P. Taberna, P. Simon, J. Power Sources 158 (2006) 571–577.
- [17] J.R. Dahn, T. Zheng, Y. Liu, J.S. Xue, Science 270 (1995) 590.
- [18] W.A. Schalkwijk, B. Scrosati, Advances in Lithium-Ion Batteries, Kluwer Academic/Plenum Publishers, New York, 2002.
- [19] T.D. Burchell, Carbon Materials for Advanced Technologies, Pergamon, Amsterdam, 1999.
- [20] D. Aurbach, B. Markovsky, I. Weissman, E. Levi, Y. Ein-Eli, Electrochim. Acta 45 (1999) 67.
- [21] E. Peled, in: J.O. Besenhard (Ed.), Handbook of Battery Materials, Wiley-VCH, Weinheim, 1999.
- [22] M. Hahn, O. Barbieri, R. Gally, R. Kötz, Carbon 44 (2006) 2523–2533.
- [23] H. Nakamura, M. Okamura, Proceedings of the thirteenth International Seminar on Double-Layer Capacitors, Florida Educational Seminars, Inc., 2003.
- [24] K. Zaghib, G. Nadeau, K. Kinoshita, J. Electrochem. Soc. 147 (2000) 2110.
- [25] V. Khomenko, V. Barsukov, Electrochim. Acta 52 (2007) 2829–2840.
- [26] N. Takami, A. Satoh, M. Hara, T. Ohsaki, J. Electrochem. Soc. 142 (1995) 371.
- [27] A. Funabiki, M. Inaba, Z. Ogumi, S. Yuasa, J. Otsuji, A. Tasaka, J. Electrochem. Soc. 145 (1998) 172.
- [28] A. Du Pasquier, A. Laforgue, P. Simon, G.G. Amatucci, J.-F. Fauvarque, J. Electrochem. Soc. 149 (2002) A302–A306.
- [29] P. Azais, L. Duclaux, P. Florian, D. Massiot, M.A. Lillo-Rodenas, A. Linares-Solano, J.P. Peres, C. Jehoulet, F. Béguin, J. Power Sources 171 (2007) 1046–1053.
- [30] B. Markovsky, Y. Talyosoff, G. Salitra, D. Aurbach, H.J. Kim, S. Choi, Electrochem. Commun. 6 (2004) 821–826.